

Experimental and Theoretical Characterization of the Crystal Structure of 4,4-dimethoxy-1,1-biphenyl (4-DMB)

N Kumari^a, A A Yadav^b, S A Sankpal^b, S Murugavel^c, D Lakshmanan^d & R Kant^{a*}

^aDepartment of Physics, University of Jammu, Jammu Tawi, Jammu & Kashmir 180 006, India

^bDepartment of Chemistry, Shivaji University Kolhapur, Maharashtra 416 004, India

^cDepartment of Physics, Thanthai Periyar Government Institute of Technology, Vellore, Tamil Nadu 632 002, India

^dDepartment of Physics, C. Abdul Hakeem College of Engineering and Technology, Melvisharam, Tamil Nadu 632 509, India

Received 23 June 2023; accepted 10 August 2023

4,4-dimethoxy-1,1-biphenyl has been synthesized and its chemical structure has been characterized by various spectroscopic techniques like FT-IR, ¹H & ¹³C NMR, and SC-XRD methods. The structure reveals the existence of two C-H... π and a weak π ... π interaction which are primarily responsible for the stability of the crystal packing. A comparison of the X-ray structure & its optimized data using DFT has been made. The frontier molecular orbital analysis (FMO) reveals an energy gap of 4.57 eV and the molecular electrostatic potential map shows the charge distribution in the molecule. The two-dimensional fingerprint maps as emanated from the Hirshfeld analysis demonstrates the presence of H...H, C...H and O...H interactions. The molecular docking analysis has also been performed with tyrosinase (3NQ1).

Keywords: X-ray structure; Density functional theory; Hirshfeld surface; Molecular docking

1 Introduction

Biphenyl has numerous applications in fields like industry, materials science, and pharmaceuticals¹⁻³. They also exhibit potent biological activities, including anti-fungal, anti-hypertensive, anti-inflammatory, anti-cancer, *etc*⁴⁻⁸. As a consequence, the search for novel biphenyl-based molecules possessing potent biological properties has become critical.

In continuation of our work on biphenyls, we present the synthesis, characterization and X-ray structure elucidation of 4,4-dimethoxy-1,1-biphenyl (4-DMB)⁹⁻¹³. The theoretical calculations have been performed by employing the Density Functional Theory (DFT) approach in an effort to experimentally and theoretically describe the crystal structure. The Hirshfeld surface analysis has been employed to explore the intermolecular interactions in the crystal structure. The molecular docking analysis has also been carried out using tyrosinase (3NQ1) to assess the therapeutic potential of 4-DMB for dermatological disorders.

2 Materials and Methods

2.1 Synthesis

10 mg of Fe₃O₄/ Pd, 4-bromoanisole (1mmol) in 3ml of water-ethanol (1:1), 4-methoxy phenylboronic

acid (1.1 mmol) and 2mmol of K₂CO₃ (0.276 mg) all were added to a round bottom flask. The resulting mixture was then stirred for 2 hours at 40 °C, while being monitored using TLC. Once the reaction was complete, ethanol (5ml) was added, and the catalyst was separated using a magnet. The purification process was accomplished by simple recrystallization. The product identified using NMR and FT-IR spectroscopic techniques.

FT-IR :3115, 2959, 2910, 2347, 1680, 1598, 1485, 1233, 1173, 1028, 813, 612 cm⁻¹.

¹H NMR: (400 MHz, CDCl₃): δ 3.85 (6H, s, -CH₃), 6.95-6.97 (4H, t, -ArH), 7.26-7.49 (4H, t, -ArH).

¹³C NMR (100 MHz, CDCl₃): δ 55.34, 114.15, 127.73, 133.47, 158.67.

2.2 Structure determination

The SC-XRD data were collected using the HyPix3000 diffractometer at 293 K using MoK α radiation. The structure has been solved by intrinsic phasing (SHELXT)¹⁴ and refined by full-matrix least squares on F² (SHELXL)¹⁵ using OLEX Software¹⁶. All hydrogen atoms were fixed and non-hydrogen atoms were allowed to refine anisotropically. The final cycle of refinement brought the residual index to 0.046. The geometrical calculations were performed using PLATON¹⁷ and PARST¹⁸ software, while the

*Corresponding author: (E-mail: rkant.ju@gmail.com)

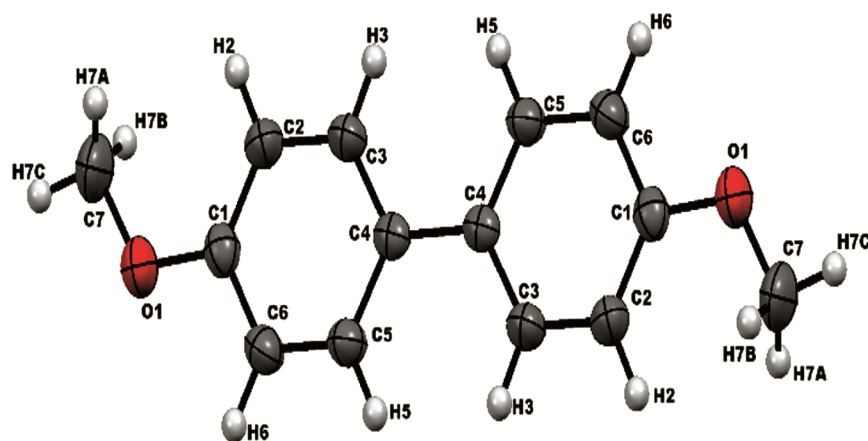


Fig. 1— ORTEP view of 4-DMB.

Table 1 — Crystal data of 4-DMB.

CCDC No.	2270742
Formula	C ₇ H ₇ O
Weight	107.13
Temperature	293(2) K
Crystal system	Orthorhombic
Spacegroup	Pbca
Cell parameters	$a=7.4305(3)\text{Å}$ $b=6.2205(2)\text{Å}$ $c=24.5507(10)\text{Å}$ $\alpha, \beta, \gamma=90^\circ$
Volume (V)	1134.77(7) Å ³
Z	8
Absorption coefficient	0.083 mm ⁻¹
F(000)	456.0
Radiation (MoK α)	0.71073 Å
Theta range	6.41°–54.832°
No. of Reflections	8819
No. of parameters	74
Index ranges	$-9 \leq h \leq 8, -7 \leq k \leq 8, -31 \leq l \leq 30$
Independent reflections	1231 [Rint = 0.0348, Rsigma = 0.0273]
Final [$I \geq 2\sigma(I)$]	R1 = 0.0466, wR2 = 0.1180
R indexes [all data]	R1 = 0.0776, wR2 = 0.1358
GOOF on F2	1.058
Largest diff. peak/hole	0.12/-0.15 e Å ⁻³

ORTEP and packing views were obtained using the MERCURY software¹⁹.

2.3 Theoretical studies

DFT method has been employed for the optimization of the structure with B3LYP/6-311G++G (d, p) basis set using Gaussian 09²⁰. The CIF file has been used as an input for the DFT calculations. The HOMO/LUMO gap and molecular electrostatic potential (MEP) map have been computed using DFT. The Crystal Explorer 21.5²¹ helped investigate the Hirshfeld surface and the 2D-fingerprint plots. The

Table 2 — Comparison of bond lengths and angles between XRD and DFT.

Bond lengths (Å)	XRD	DFT
O1-C7	1.418	1.420
C1-C2	1.375	1.395
C1-C6	1.377	1.398
C4-C3	1.388	1.401
O1-C1	1.369	1.364
C2-C3	1.380	1.394
C6-C5	1.375	1.384
C4-C5	1.392	1.409
Bond angles (°)	XRD	DFT
C1-C2-C3	119.80	119.89
C2-C3-C4	122.81	122.57
C3-C4-C5	115.81	116.06
C4-C5-C6	120.00	122.22
C5-C6-C1	120.71	120.43
O1-C1-C6	116.02	116.20
O1-C1-C2	125.10	124.97
C1-O1-C7	118.00	118.46
C6-C1-C2	118.87	118.81

molecular docking has been performed using the AutoDock Vina software²² for the target protein tyrosinase (PDB ID: 3NQ1) having interaction with the ligand (4-DMB) for visualising the ligand-protein binding sites using Discovery Studio 4.1 Visualizer software^{23,24}.

3 Results and discussion

3.1 X-ray structure analysis

The crystal belongs to the monoclinic system having space group Pbca and the precise crystal data are presented in Table 1. The asymmetric unit contains half of the molecule and the remaining fragment was grown (ORTEP Fig. 1). The geometrical parameters obtained experimentally were optimized using DFT formalism and it shows a fair amount of agreement (Table 2).

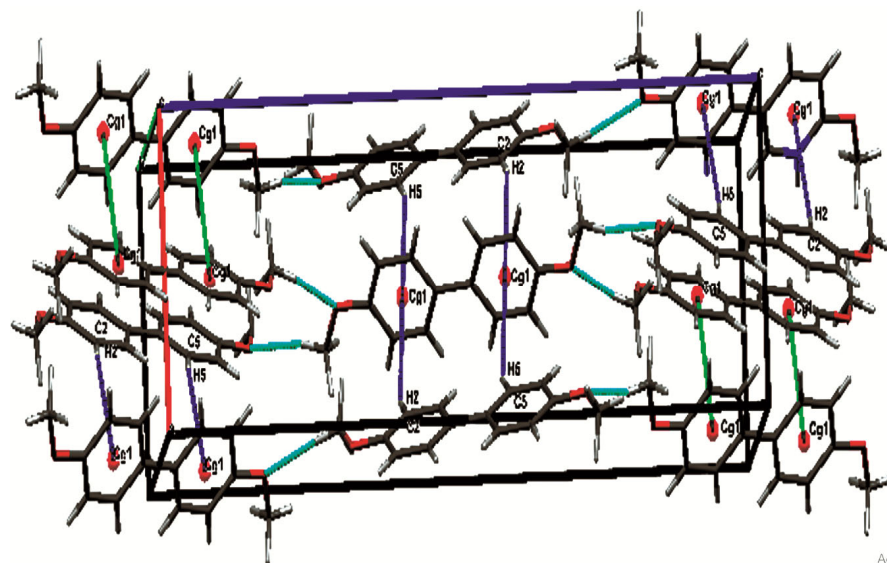


Fig. 2— Packing view with C7-H7-O1 (turquoise), C-H...Cg (blue) and Cg...Cg (green) interactions.

Table 3 — Different interactions of 4-DMB.

D-H...A	D-H (Å)	H...A (Å)	D...A (Å)	D-H...A (°)
C7-H7C-O1	0.94	2.62	3.47	144.9
C2-H2-Cg1 ⁱ	0.93	2.86	3.652	138
C5-H5-Cg1 ⁱⁱ	0.93	2.82	3.615	139.3

i= 1/2 -X, 1/2 +Y, Z

ii= 3/2-X, -1/2 +Y, Z

Table 4 — Chemical reactivity parameters.

Parameters	(eV)
$E_{\text{HOMO}}, E_{\text{H}}$	-5.49
$E_{\text{LUMO}}, E_{\text{L}}$	-0.91
Energy gap, $\Delta E = E_{\text{H}} - E_{\text{L}} $	4.58
Ionisation potential, $-E_{\text{H}}$	5.49
Electron affinity, $-E_{\text{L}}$	0.91
Chemical Potential, $\mu = -\chi$	-3.2
Electronegativity, $\chi = -(E_{\text{H}} + E_{\text{L}})/2$	3.2
Softness, $\sigma = 1/2\eta$ (eV) ⁻¹	0.22
Hardness, $\eta = E_{\text{H}} - E_{\text{L}} /2$	2.29
Global Electrophilicity, $\omega = \mu^2/2\eta$	2.23

Different interactions of 4-DMB are shown in Table 3. There exists a C-H...O and two C-H... π interactions, besides a weak Cg...Cg interaction (distance 4.825Å, symmetry code: 3/2-X, 1/2+Y, Z). The packing view of the molecule is shown in Fig. 2.

3.2 HOMO/LUMO and MEP analysis

The energies of HOMO and LUMO as computed using DFT are: $E_{\text{HOMO}} = -5.48$ eV and $E_{\text{LUMO}} = -0.912$ eV, respectively (Table 4). The energy difference (4.57 eV) between the two is relatively large, meaning that the molecule is hard and chemically stable

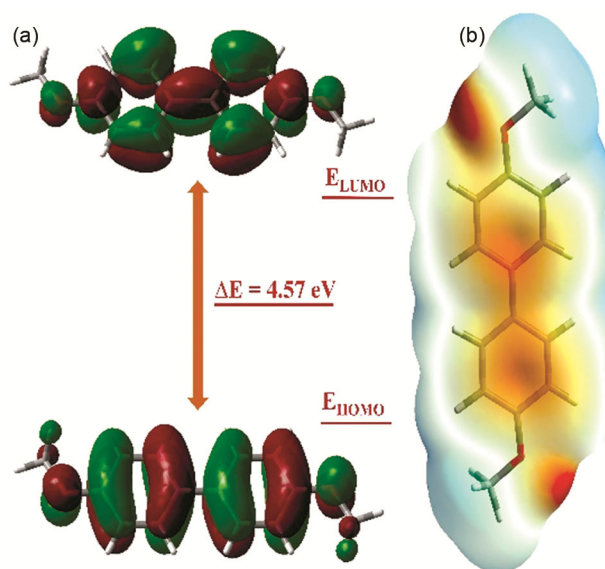


Fig. 3 — (a) HOMO/LUMO (b) MEP map of 4-DMB.

(Fig. 3(a)). The positive (blue) potential region in the MEP plot is concentrated more over the hydrogen atoms, while the negative (red) potential region is over the oxygen atom. The pale-yellow region indicates the existence of significant C-H... π interactions (Fig 3b).

3.3 Hirshfeld surface analysis

The Hirshfeld surface of the molecule mapped over the d_{norm} is shown in Fig. 4²¹. The d_{norm} value is positive for shorter contacts (blue region), negative for the longer contacts (red regions) and zero in the case of van der Waals (vdW) separation²⁵. The red spots on the d_{norm}

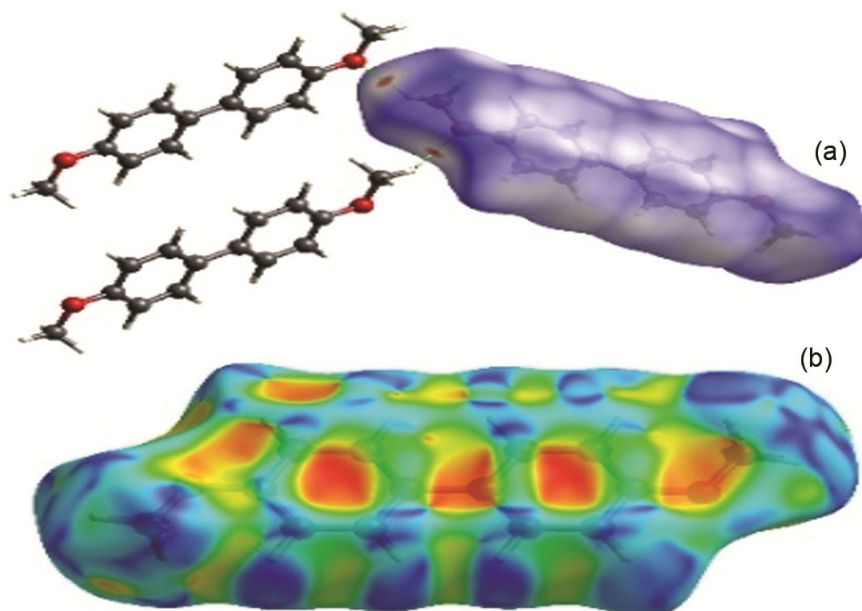


Fig. 4 — (a) d_{norm} (b) shape index plot of 4-DMB.

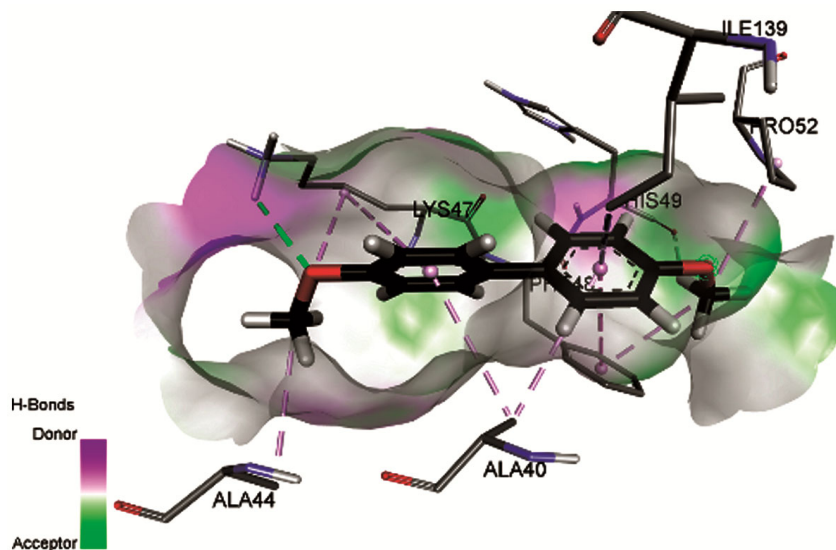


Fig. 5— Three-dimensional binding pose of 4-DMB and 3NQ1.

surface are attributed to the existence of C7–H7b...O1 (C–H...O) short contact (Fig. 4(a)) whereas the C–H... π interactions are indicated by red patches on the shape index plots (Fig. 4(b)). The contributions from different contacts to the total Hirshfeld surface areas as obtained using the fingerprint plot are: O...H (14.8%), H...H (47.3%) and C...H (37.9%).

3.4 Molecular docking analysis

The three-dimensional binding pose of 4DMB at the binding site of the 3NQ1 enzyme is shown in Fig. 5. The 4-DMB:3NQ1 complex is stabilized by one conventional hydrogen bond, one carbon-

hydrogen bond and eight hydrophobic bonds. The conventional hydrogen bond exists between the donor hydrogen atom of the residue LYS47 and the oxygen atom of 4-DMB at a distance of 2.45 Å. The carbon-hydrogen bond exists between the donor hydrogen atom of 4-DMB and the oxygen atom of the residue HIS49 at a distance of 3.11 Å. The binding energy (B.E), distance and bonding type of the eight hydrophobic bonds are listed in Table 5, respectively. The binding energy score of -7.8 Kcal/mol for the 4-DMB:3NQ1 complex confirms that 4-DMB has the potential to act as a potent inhibitor for tyrosinase.

Table 5 — Different types of interactions between 4-DMB and 3NQ1.

Inhibitor	B.E (Kcal mol ⁻¹)	Interactions	Distance (Å)	Bonding	Bonding Types
4-DMB	-7.8	LYS47[H...O]	2.45	Hydrogen Bond	Conventional Hydrogen Bond
		HIS49[O...H]	3.11	Hydrogen Bond	Carbon Hydrogen Bond
		ILE139[CH...π]	3.54	Hydrophobic	Pi-Sigma
		PHE48[π...CH]	3.80	Hydrophobic	Pi-Sigma
		PHE48[π...π]	4.12	Hydrophobic	Pi-Pi Stacked
		ALA44 [π...C]	4.12	Hydrophobic	Alkyl
		LYS47 [π...C]	4.82	Hydrophobic	Alkyl
		PRO52 [π...C]	3.89	Hydrophobic	Alkyl
		ALA40[C...π]	4.41	Hydrophobic	Pi-Alkyl
		ALA40[C... π]	4.20	Hydrophobic	Pi-Alkyl

4 Conclusion

The structure of 4-DMB has been validated using spectroscopic and X-ray diffraction techniques. The crystal structure has C-H...π and π...π interactions that stabilize the crystal packing. A DFT calculation infers that the theoretically predicted structural values are in good agreement with the experimental values. The HOMO–LUMO energy gap of the molecule is 4.57 eV and it confirms the stability of the compound. The MEP map shows that the oxygen atoms present in the molecule exhibit electrophilic nature and hydrogen atoms are nucleophiles. The two-dimensional fingerprint plot analysis indicates that H...H contacts have a substantial impact on the Hirshfeld surface as a whole. The analysis of the molecular docking with the complex 4-DMB:3NQ1 shows a very good binding energy -7.8 kcal/mol and may be considered as an efficient inhibitor for tyrosinase.

Declaration

Authors declare that there is no conflict of interest.

References

- Reddy A L V K & Kathale N E, *Orient J Chem*, 33 (2017) 971.
- Jain Z S, Gide P S & Kankate R S, *Arab J Chem*, 10 (2017) S2051.
- Ghasemi S, Sharifi S & Mojarrad J S, *Adv Pharm Bull*, 10 (2020) 423.
- Cincinelli R, Zwick V, Musso L, Zuco V, De Cesare M, Zunino F, Simoes-Pires C, Nurisso A, Giannini G, Cuendet M & Dallavalle S, *Eur J Med Chem*, 112 (2016) 99.
- Lee C Y, Choi H, Park E Y, Nguyen T T, Maeng H J, Mee Lee K, Jun H S & Shin D, *Chem Biol Drug Des*, 98 (2021) 733.
- Pisano M, Dettori M A, Fabbri D, Delogu G, Palmieri G & Rozzo C, *Int J Mol Sci*, 22 (2021) 5636.
- Zhao D, Zhao S, Zhao L, Zhang X, Wei P, Liu C, Hao C, Sun B, Su X & Cheng M, *Bioorg Med Chem*, 25 (2017) 750.
- Chinnamanyakar R & Ramanathan E M, *Biointerface Res Appl Chem*, 11 (2021) 8266.
- Rajnikant, Watkin D J & Tranter G, *Acta Crystallogr*, C51 (1995) 2161.
- Rajnikant, Dinesh & Singh D, *Bull Mater Sci*, 27 (2004) 31.
- Rajnikant & Watkin D J, *Acta Crystallogr*, C51 (1995) 2388.
- Kumari N, Sharma R, Singh M & Kant R, *Chem Pharm Res*, 4 (2022) 1.
- Kumari N, Sharma R, Yadav A A, Sankpal S A, Raj J M, Murugavel S & Kant R, *Eur J Chem*, 14 (2023) 90.
- Sheldrick G M, *Acta Crystallogr*, A64 (2008) 112.
- Sheldrick G M, *Acta Crystallogr*, A71 (2015) 3.
- Dolomanov O V, Bourhis L J, Gildea R J, Howard J A K & Puschmann K, *J Appl Crystallogr*, 42 (2009) 339.
- Spek A L, *Acta Crystallogr*, D65 (2009) 148.
- Nardelli M, *Comput Chem*, 7 (1983) 95.
- Macrae C F, Bruno I J, Chisholm J A, Edgington P R, McCabe P, Pidcock E, Rodriguez-Monge L, Taylor R, Streek J V & Wood PA, *J Appl Crystallogr*, 41 (2008) 466.
- Frisch M J, Trucks G W, Schlegel H B, Scuseria G E, Robb M A, Mennucci B, Petersson G A, Nakatsuji H, Caricato M & Li X, *Gaussian 09, Revision C.01* (Wallingford, CT: Gaussian, Inc, 2009).
- Spackman P R, Turner M J, McKinnon J J, Wolff S K, Grimwood D J, Jayatilaka D & Spackman MA, *J Appl Crystallogr*, 54 (2021) 1006.
- Morris G M, Huey R, Lindstrom W, Sanner M F, Belew R K, Goodsell D S & Olson A J, *J Comput Chem*, 30 (2009) 2785.
- www.rcsb.org/pdb.
- Dassault Systemes BIOVIA, [Discovery Studio 4.1 Visualizer], San Diego: Dassault Systemes, (2014).
- Prabhuswamy A, Mohammed Y H, Al-Ostoot F H, Venkatesh G D, Anandalwar S M, Khanum S A & Krishnappagowda L N, *Eur J Chem*, 12 (2021) 304.